JOURNAL OF GEOPHYSICAL RESEARCH, VOL. 98, NO. A7, PAGES 11,567–11,579, JULY 1, 1993

Evidence for Non-Local-Thermodynamic-Equilibrium Rotation in the OH Nightglow

W. R. PENDLETON, JR., P. J. ESPY, AND M. R. HAMMOND

Department of Physics and Space Dynamics Laboratory, Utah State University, Logan

Improved ground-based Fourier transform infrared spectroscopic measurements of the OH Meinel (M) $\Delta v = 2$ and 3 nightglow emissions revealed unexpectedly intense transitions from high rotational levels. The rotational development in the P branches of the OH M (3,1), (6,3), and (7,4) bands has been followed to the $P_1(N'')$ transitions with $N'' = 10$, 12, and 13, respectively. These measurements indicate that ~10% of the OH(X, $v' = 7$) column rotational population is typically in rotational levels with $N' \geq 7$, in sharp contrast with the corresponding local thermodynamic equilibrium estimate of ~1%. The excess high-N' population also persists in the lower vibrational states of OH(X), as evidenced by the readily detectable high-$P_1(N'')$ transitions in the (3,1) and (6,3) bands and by the presence of observable R branch heads in the (4,2) and (5,3) bands. The R heads in the (4,2) and (5,3) bands form at moderately high N' and are typically much more intense than expected on the assumption of complete rotational-translational equilibration throughout the OH M source region. These new results provide strong evidence for incomplete R-T equilibration of OH($X^2\Pi$, $3 \leq v' \leq 7$, J') on a column basis under typical nightglow conditions.

1. INTRODUCTION

The discovery of the vibration-rotation bands of the OH radical in the night airglow by *Meinel* [1950*a*,*b*] was rapidly followed by the implementation of procedures for extracting a "spectroscopic rotational temperature" (T_r) from the rotational distribution of the emission within a specific band [*Meinel*, 1950*c*]. Initially, interest in this parameter stemmed from the possibility that it might be indicative of the height of the source region or, conversely, that the establishment of the emission height by other means might render T_r a useful thermal diagnostic for this atmospheric region [*Chamberlain*, 1961].

As noted by *McPherson and Vallance Jones* [1960], the interpretation of T_r is clearly dependent upon whether the vibrationally excited OH(X) molecules attain rotational-translational (R-T) equilibrium before emitting. Initial theoretical assessments of possible R-T equilibration suffered from several significant uncertainties. In particular, considerable uncertainty was attached to each of the following important considerations: (1) the nascent distribution of OH(X,v',N') in the source region; (2) the height of the source region; (3) the radiative lifetimes of the excited OH(X,v') molecules; and (4) the R-T relaxation properties of OH(X,v',N') in collisions with other atmospheric species. Despite these uncertainties, initial considerations yielded the "fairly safe" conclusion that below about 90 km the parameter T_r should be equal to the local gas-kinetic temperature [*McPherson and Vallance Jones*, 1960]. This view was supported by *Wallace* [1962] who discussed additional evidence for its validity.

Most of the early experimental investigations of the rotational distribution of OH(X,v') in the nightglow were restricted to rather weak high-overtone emissions in the visible and photographic IR extending to about 9000 Å. These higher overtone bands occur in a region of significant background emission, which includes the nightglow continuum. Thus high-precision determinations of the relative rotational populations were typically limited to the first few rotational levels, and even for these the accuracy was suspect as a result of poorly defined transition probabilities (line strengths) which did not account for vibrational-rotational interactions. Perhaps the most critical early assessments of the OH (X,v',N') rovibrational population distributions in the nightglow were those of *Shefov* [1961] who concluded that significant deviations from an isothermal Boltzmann distribution (IBD) are typically limited to rotational levels with $N' > 5$ and then only for OH M bands from the higher vibrational levels. However, *Shefov* [1972*a*,*b*] later suggested that these higher-N' deviations were unreliable as a result of inadequate signal-to-noise and signal-to-background in the measurements. The intensity factors of *Benedict et al.* [1953], in which the vibration-rotation interaction was neglected, were used in these early analyses.

Subsequently, in the early 1970s, some measurements of the OH Meinel nightglow rotational intensity distributions, using relatively coarse spectral resolution, suggested the possibility that the assumption of an IBD in rotation might not be valid even for levels with $N' < 6$ under all geophysical conditions [*Harrison et al.*, 1970; *Harrison et al.*, 1971; *Gattinger and Vallance Jones*, 1973]. These observations prompted a more detailed examination of the R-T relaxation problem as it applies to the OH M nightglow [*Nicholls*, 1971; *Nicholls et al.*, 1972]. However, the lack of definitive input information for the relaxation model resulted in somewhat tentative conclusions regarding the extent of the R-T relaxation expected on a column basis. In a subsequent review of the available evidence, *Vallance Jones* [1973] concluded that the reported rotational distribution anomalies in the OH Meinel nightglow had not been firmly established. This conclusion was based, in part, on the observation that spectral data obtained at significantly higher resolution [*Dick*, 1972; *Shefov*, 1972*a*; *Harrison and Kendall*, 1973] did not seem to reveal such abnormalities. *Lewellyn and Long* [1978] used improved input information in a R-T relaxation model and suggested the possibility of non-local thermodynamic equilibrium (NLTE) rotation of vibrationally excited OH(X) in the upper regions of the concentration height profile.

Several data sets which bear on the question of Boltzmann equilibrium among the rotational levels of OH(X,v') under nightglow conditions have been published. [See, e.g., *Shefov*, 1961; *Kvifte*, 1961; *Dick*, 1972; *Sivjee et al.*, 1972; *Harrison and Kendall*, 1973; *Turnbull and Lowe*, 1983; *Sivjee and*

Paper number 93JA00740.
0148-0227/93/93JA-00740$05.00

Hamwey, 1987; *Pendleton et al.*, 1989*a*.] These measurements have clearly demonstrated that the population distributions involving the lowest rotational levels of OH(X,v') are typically described by a Boltzmann formula to within the uncertainties imposed primarily by signal-to-noise limitations and background corrections. However, the high-precision measurements of the OH M (6,2) and (8,3) rotational distributions by *Sivjee and Hamwey* [1987] suggested a significant departure from an IBD for $P_1(N'')$ transitions with $N'' = 5$ and 6 under some conditions.

Very recently improved FTIR spectroscopic measurements of the OH M nightglow emissions in the $\Delta v = 2$ and 3 sequences under conditions of high S/N and signal-to-background have revealed unexpectedly intense emission from high-N' levels associated with the (7,4) band [*Pendleton et al.*, 1989*a*]. In particular, it was demonstrated that the emission rates in the $P(12)$ and $P(13)$ transitions in the (7,4) band exceeded, under the experimental conditions, the Boltzmann values, based on the low-N' distribution, by factors of the order $x10^3$ and $x10^4$, respectively. This degree of excess emission from the high-N' rotational levels is much larger than that expected for an extended emission layer in a nonisothermal region when currently available information is used in the estimate. (It should be noted that this disparity also greatly exceeds effects introduced by set-to-set differences in the available transition probabilities.) Hence it was suggested that the high rotational levels of OH(X,$v' = 7$) in the nightglow are not in local thermodynamic equilibrium throughout the emitting region. This suggestion is supported by the recent OH M (7,3) nightglow measurements of *Perminov et al.* [1991] who report detectable nonequilibrium in upper rotational levels $6 \le N' \le 9$.

Unfortunately the OH *M* (7,4) observations of *Pendleton et al.* [1989*a*] did not permit a convenient determination of the emission rates associated with the $P(N'')$ transitions with N'' in the range $7 < N'' < 12$ as a result of severe blending of these transitions with the rotational structures of the O_2 infrared atmospheric (0,0) band and/or the OH M (8,5) band. Thus the "breaking away" of the rotational population distribution from the quasi-Boltzmann, low-N'' behavior was not well established by the observations. This point is important since the departure of the observed distribution from that of an IBD may reflect both non-LTE effects and temperature gradients through the source region, as noted by *Harrison et al.* [1971] and by *Shefov* [1972*a*]. Recent interest in the possible use of the departure of OH(X,v') rovibronic population distributions from an isothermal Boltzmann distribution to "probe" the effective temperature gradient through the OH Meinel nightglow source region [*Schubert and Walterscheid*, 1988; *Schubert et al.*, 1990] suggests the desirability of evaluating, to the extent possible, the relative contributions of incomplete R-T relaxation and temperature gradients to the observed behavior.

In an effort to minimize the impact of temperature gradients on the OH(X,v') rotational distributions measured in the nightglow, we have included in our analyses some spectral data sets obtained under "dynamically quiet" high-latitude winter conditions. The extensive Na-lidar measurements at 69° N during the winters of 1985-1986 and 1986-1987 by *Neuber et al.* [1988] have demonstrated that the mean temperature gradient through the OH M source region is typically only $\langle dT/dz \rangle \sim -1$ K/km under these conditions. However, the instantaneous gradient may, of course, be significantly larger under "dynamically active" conditions as a result of perturbations on the mean state resulting from wave activity and associated phenomena.

In the present paper, we extend the OH M (7,4) nightglow observations of *Pendleton et al.* [1989*a*] to high-N' emissions from other vibrational levels of OH(X,v'). In particular, we have followed the rotational development in the P branches of the (3,1) and (6,3) bands to the $P_1(N'')$ Λ-doublets with $N'' = 10$ and 12, respectively, and have observed relatively prominent R heads in the (4,2) and (5,3) bands. The (4,2) and (5,3) R heads reflect transitions from upper states with rotational quantum numbers in the range 9 - 11 and are expected to be virtually undetectable under conditions of complete R-T equilibrium at typical near-mesopause temperatures. These and related results are presented, and some of their implications are discussed.

2. EXPERIMENTAL

2.1. *Instrumentation*

The technique of Fourier transform infrared spectroscopy with a field-widened Michelson interferometer was used in this study. The interferometer is a modified version of the instrument described in detail by *Haycock and Baker* [1974]. Design criteria for this type of Michelson interferometer have been discussed by *Steed* [1979], and a useful review of field-widened interferometers for Fourier spectroscopy has been presented by *Baker* [1977].

In the present application, the optical head of the interferometer was mounted in a field-operational environmental enclosure [*Steed et al.*, 1981]. More recently, temperature stabilization ($\Delta T \approx \pm 0.1$ K) of critical optical components of the interferometer has resulted in greatly improved long-term alignment stability and has simplified the wave number and responsivity characterizations of the instrument for co-added spectra [*Pendleton et al.*, 1989*b*].

A liquid-nitrogen-cooled intrinsic germanium detector (RCA Ltd.) with an effective diameter of ≈5.0 mm and a NEP of $\approx 10^{-14}$ W/Hz$^{1/2}$ at ≈7000 cm^{-1} (1.43 μm) provided good IR sensitivity in the spectral range 6250 - 10,000 cm^{-1}. In this operating mode, the NESR of the interferometer is typically about 4 x 10^{-14} W cm^{-2} sr^{-1}/cm^{-1} at 7000 cm^{-1} when using a 25-s retardation scan [*Steed and Baker*, 1979], which corresponds to ≈4 R/cm^{-1} or ≈2 R/Å. An unapodized spectral resolution of 1.7 cm^{-1} is realized for normal operating conditions. Hence a system NER of <10 R is typical in the 7000-cm^{-1} region. As a point of reference, the $P_1(3)$ Λ-doublet (≈6522 cm^{-1}) in the OH M (3,1) band, which is the most intense P_1 branch transition under average ($T_r \approx 200$ K) nightglow conditions, is characterized by an apparent column emission rate (zenith) of about 7 kR. (This figure is based on I(3,1) ≅ 54 kR [*Bates*, 1982] and f[$P_1(3)$] ≅ 13% at 200 K from our measurements.) Thus this transition is normally detected with a S/N ratio of several hundred in single scans.

Individual quasi-single-sided interferograms are recorded at the rate of ≈3/min using a maximum optical retardation commensurate with a resolving power of nominally 4 x 10^3 at 10,000 cm^{-1} (1 μm) in the transformed spectra. The procedures currently used to obtain spectra from the raw interferograms have been described by *Espy et al.* [1988] and by *Pendleton et al.* [1989*b*]. The Kaiser-Bessel apodization function normally used in processing the interferograms yields the approximation to the instrumental line shape (ILS) illustrated in Figure 1. The

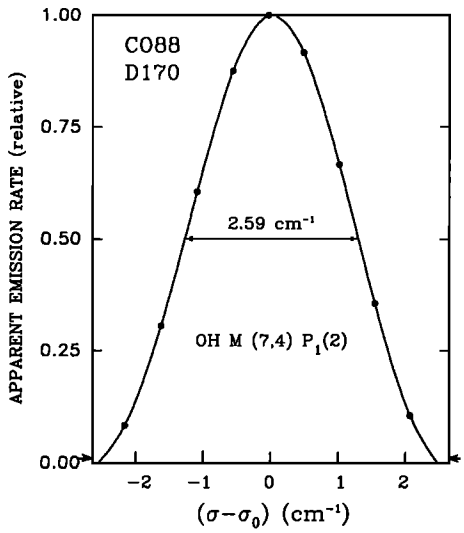

Fig. 1. Instrumental line shape function associated with a "soft" Kaiser-Bessel apodization. The arrows near the bottom of the figure identify the level (<0.01) of the principal sidelobe (not shown).

distribution in the figure actually reflects the instrumental response to the $P_1(2)$ Λ-doublet in the OH M (7,4) band. However, the $P_{1e}(2)$ - $P_{1f}(2)$ separation is only $\approx$0.12 cm^{-1} [*Coxon*, 1980; *Coxon and Foster*, 1982], or roughly 5% of a resolution element. As a result, the true ILS differs almost imperceptibly from the distribution in the figure. It should be It should be noted that this ILS is characterized by a full width at half maximum (FWHM) of $\approx$2.6 cm^{-1} and principal side lobe with a peak amplitude $<10^{-2}$ that of the central maximum. The distant side lobes decrease at the rate $\approx$6 db/octave.

In the case of coherently summed nightglow spectra, a S/N ratio of $\sim 10^4$ has been realized for the previously mentioned "reference transition," the OH M (3,1) $P_1(3)$ Λ-doublet. Under these conditions, a "harder" Kaiser-Bessel apodization has been employed to reduce the amplitude of the principal side lobe in the ILS to $\approx 10^{-3}$ that of the central maximum. Thus reliable detection and quantitative measurement of relatively weak emission features (~100 R) occurring near the intense principal OH M airglow transitions becomes possible when the "harder" apodization is utilized.

2.2. *Relative Rotational Populations*

The relative column populations of OH($X^2\Pi$,v',J') were extracted from the instrument-corrected apparent relative column emission rates (CER) using available transition probabilities for the pertinent OH M vibration-rotation transitions. Under typical experimental conditions, the OH M P branch spin doublets [$P_1(N'')$ and $P_2(N'')$] were highly resolved for low N'' and adequately resolved for the highest-N'' spin doublets utilized in the study. For example, the $P_1(2)$ - $P_2(2)$ separation in the (7,4) band is $\approx$22 cm^{-1}; whereas, the $P_1(13)$ - $P_2(13)$ separation is $\approx$5.7 cm^{-1}. Both of these intervals are significantly larger than the experimental resolution of $\approx$2.6 cm^{-1}. The high-$P(N'')$ transitions were observed with a very satisfactory S/N ratio, as illustrated in Figure 2 for the OH M (7,4) $P(13)$ transitions. The broadening of the high-N'' peaks resulting from the finite separation of the Λ-doublet components is also illustrated in the figure.

In most cases, the more intense $P_1(N'')$ components of the spin doublets were utilized in the rotational population determinations. Each $P_1(N'')$ peak in the spectrum reflects an unresolved Λ-type doublet, as previously noted. The separation of the components in the Λ-doublets increases significantly with increasing rotation. For example, in the case of the OH M (7,4) band, the Λ-doublet separation is $\approx$0.12 cm^{-1} for the $P_1(2)$ transitions and about 2 cm^{-1} for the $P_1(13)$ transitions [*Coxon*, 1980; *Coxon and Foster*, 1982]. Thus the Λ-doublet separation is small compared to the instrumental width ($\approx$2.6 cm^{-1}) for $P_1(N'')$ transitions with N'' small, but this separation approaches the instrumental width for the $P_1(N'')$ transitions with N'' relatively large.

In view of the instrumentally significant Λ-doublet separations for the high-N'' transitions, the area under each $P_1(N'')$ spectral peak was used in the relative population determinations. This procedure is expected to eliminate the systematic error associated with the use of peak amplitudes under conditions where the low-N'' Λ-doublet peaks closely reflect the true ILS, whereas the high-N'' peaks are systematically broader than the ILS as a result of the rapid N'' dependent increase in the separations of the spectrally unresolved Λ-doublets.

The column emission rate (CER) in a specific OH($X^2\Pi$) Λ-doubled vibration-rotation transition $(i', v', J') \rightarrow (i'', v'', J'')$ is expressed in the form

$$\begin{aligned} &\mathrm{CER}(i', v', J', \rightarrow i'', v'', J'') = \\ &\overline{\mathrm{A}}(i', v', J' \rightarrow i'', v'', J'')\, N(i', v', J'), \end{aligned} \tag{1}$$

where $\overline{\mathrm{A}}$ is an appropriate Einstein coefficient [*Mies*, 1974; *Langhoff et al.*, 1986; *Turnbull and Lowe*, 1989; *Nelson et al.*, 1990] and N is the column population of molecules in the upper level. Conventionally, $i' = 1 = i''$ for the principal vibration-rotation transitions associated with OH($X^2\Pi_{3/2}$).

The uncertainties in the determinations of relative rotational populations resulting from an imperfect knowledge of the J' dependence of the relative Einstein A coefficients is illustrated in Figure 3. In this figure, the J' dependencies of available sets of A coefficients for the P_1 branch transitions in the OH M (7,4) band are compared by normalizing the sets at $J' = 1.5$. (It is of interest to note that the various absolute values for the $P_1(J' = 1.5)$ transition probability differ by as much as a factor of 2.1.) The set designated by the open diamonds is based on the OH M rotational line strengths for intermediate

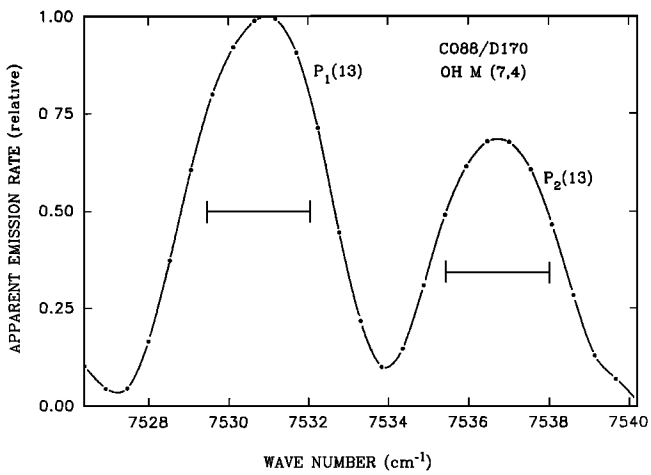

Fig. 2. Illustration of the high S/N ratio realized in observations of the OH M (7,4) $P(13)$ transitions in the night airglow under mid-latitude, summer conditions. The horizontal bars define the instrumental width of Figure 1.

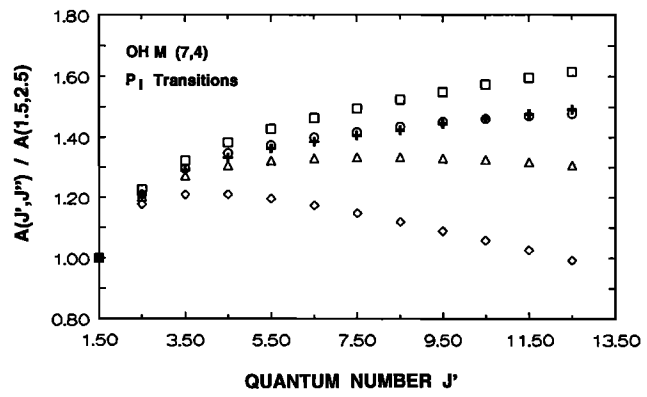

Fig. 3. A comparison of the J' dependence of available OH M (7,4) P_1-branch Einstein A coefficients. Each set is normalized to unity at $J' = 1.5$. [*Benedict et al.*, 1953 (open diamonds); *Mies*, 1974 (pluses); *Langhoff et al.*, 1986 (open squares); *Turnbull and Lowe*, 1989 (open triangles); *Nelson et al.*, 1990 (open circles)]

coupling (Hill and Van Vleck (HVV) approximation) of *Benedict et al.* [1953], which apply strictly to only the (0,0) band of a $^2\Pi$ (inverted) - $^2\Pi$ (inverted) transition since the same value of the parameter Y_0 [= (A_0/B_0) = -7.48] was used for upper and lower vibrational states. However, we have computed HVV line strengths for the OH M (7,4) $P_1(N")$ transitions of interest using the optimum OH($X^2\Pi,v' \leq 10$) molecular constants of *Coxon* [1980] and *Coxon and Foster* [1982] and find these more refined line strengths to differ by <1% from those of BPH. The BPH coefficients, which were used extensively for interpreting OH M airglow measurements during the period 1953-1974, do not include effects resulting from the interaction of vibration with rotation. Hence the $P_1(J')$ probabilities are much smaller at high J' than those which account, at least approximately, for the impact of the vibration-rotation interaction.

It is clear from the figure that the OH M (7,4) P_1 branch A coefficients of *Mies* [1974] and *Nelson et al.* [1990] exhibit nearly the same J' dependence, whereas those of *Langhoff et al.* [1986] and *Turnbull and Lowe* [1989] exhibit a stronger and weaker J' dependence, respectively. Since it is not currently possible to unequivocally choose one of these four sets as being "correct," a J' dependent uncertainty in determinations of $N(i',v',J')$ results. This uncertainty varies from a few percent at low J' to about 20% (± 10% from mean) at $J' = 12.5$, the largest J' value of interest to our measurements.

The apparent CER measured with a ground-based instrument differs from the true CER as a result of atmospheric extinction effects. In the determination of true relative column populations, the apparent CERs must be corrected for differential extinction, which is dominated by molecular absorption for the conditions of interest. Clearly, both components of a Λ-doublet must generally be considered in evaluating the effective atmospheric extinction as a result of the high degree of spectral variability in atmospheric transmittance.

For the OH M transitions and data sets used in this study, the estimated corrections for differential attenuation by the atmosphere were ≤15%. The largest corrections were applied to the OH M (7,4) $P_1(12)$ and $P_1(13)$ transitions under mid-latitude summer conditions where a typical column density of H_2O [CD(H_2O)] for a vertical path to space from the measurement altitude of ≈3 km was estimated to be ≈3 x $10^{22}/cm^2$. The estimates of CD(H_2O) were based on observed relative attenuation of selected OH M transitions using the procedures outlined by *Turnbull and Lowe* [1983] and by *Roychoudhury* [1983]. For the high-latitude winter measurements, no corrections were applied since the estimated CD(H_2O) of typically ≲3 x $10^{21}/cm^2$ rendered such corrections insignificant.

3. OBSERVATIONS

3.1. General

Observations of OH M $\Delta v = 2$ and 3 nightglow emissions were acquired primarily for two distinct geographical/seasonal conditions: (1) high-latitude/winter (HLW) and (2) mid-latitude/summer (MLS). The high-latitude sites included the Poker Flat Research Range (65.1° N; 147.5° W) near Fairbanks, Alaska and Nordlysstajonen (78.5° N; 15.1° E) near Longyearbyen, Svalbard. The mid-latitude observations were made from the Institute for Alpine and Arctic Research (INSTAAR) (40.0° N; 105.6° W) near Boulder, Colorado. The INSTAAR facility is located at an altitude of ≈3.0 km; whereas the high-latitude sites are located near sea level.

The HLW observations are of special interest for at least two reasons: (1) the OH M source region is on average expected to be nearly isothermal [*Neuber et al.*, 1988], and (2) atmospheric absorption by water vapor in the lower troposphere is at times greatly reduced as a result of low temperatures (≈-40° C at ground level). The almost isothermal nature of the source region is expected to facilitate the investigation of NLTE effects in the OH(X,v') rotational distribution since the magnitude of these effects is much greater than uncertainties introduced by the available relative transition probabilities. Also, greatly reduced water-vapor absorption facilitates the investigation of certain OH M bands which occur in the wings of H_2O absorption bands. In particular, the high-$N"$ P branch transitions in the OH M (7,4) band appear in the "blue" wing of the Ψ band of H_2O; whereas, the (6,3) band appears in the "red" wing of the Φ band.

The MLS observations provide the opportunity to study the OH M rotational development under conditions where the source region is frequently much cooler than is typical of HLW conditions. This point is deemed significant since under the assumption of LTE throughout the source region the population in the high rotational levels ($N' \gtrsim 10$) is expected to change markedly relative to that in the low rotational levels from HLW to MLS conditions. For example, the LTE population ratio [OH($X,v' = 7,N' = 12$)] / [OH($X,v' = 7,N' = 1$)] varies from ≈1 x 10^{-7} for a fairly common MLS mesopause temperature of 170 K to ≈7 x 10^{-6} for a common HLW source-region temperature of 220 K. Thus this population ratio is expected to change by a factor of roughly 70 if LTE conditions prevail for rotation of OH($X,v' = 7$) in an isothermal source region. However, it should be noted that both of these ratios suggest levels of OH M (7,4) $P(13)$ emission below our threshold for detection since the S/N ratio for the $P_1(2)$ transition is ~10^3 in typical co-added spectra. In sharp contrast, we find the designated population ratio in column to be ~10^{-2} under both HLW and MLS conditions, as discussed in the following subsection.

3.2. OH M (7,4) Band

The rotational development in the P branches of the OH M (7,4) band has been followed through the $P(13)$ spin doublet

under both HLW and MLS conditions. A fairly typical result for HLW conditions has previously been reported by *Pendleton et al.* [1989*a*]. Here we present complementary MLS observations and compare them with the HLW results. A spectrum of the night airglow in the 7200-8400 cm^{-1} region, obtained under "dynamically quiet" mid-latitude spring-summer (June 19, 1988) conditions, is presented in Figure 4. The OH M emission levels were relatively low on this occasion. Also, the OH M rotational temperatures suggested little or no wave activity during the night, as illustrated in Figure 5. The OH M (7,4) T_r results in the figure reflect a 5.4-min sample interval which, under the given conditions, corresponds to a measurement uncertainty (statistical) of ≈ ± 1K for each sample. This evidence for low wave activity is supported by low-light-level OH M imaging measurements which revealed no discernible structure during the night [*M. J. Taylor*, private communication].

The OH M (7,4) and (8,5) bands dominate the spectral region in Figure 4, but relatively weak O_2 IR At (0,0) emission is readily identified near 7870 cm^{-1}. The zenith angle for these measurements was ≈ 67°. Thus the OH M signals were enhanced relative to the zenith levels by the van Rhijn effect (enhancement factor ≈2.5), whereas the level of the O_2 IR At (0,0) signal of interest was reduced by the dominance of increased self-absorption. As a result, the spectrum in the figure is well suited for use in determining the rotational distribution of OH($X^2\Pi$,v' = 7).

In Figure 4, the OH M (7,4) $P(13)$ transitions are identified by the arrow near 7530 cm^{-1}. These transitions, which provide the most compelling evidence for incomplete R-T relaxation of OH($X^2\Pi$,v' = 7) under typical MLS conditions, have already been presented in more detail in Figure 2. The relatively high S/N for these features coupled with the very low background yield an apparent high-N'/low-N' column emission rate (CER) ratio with an uncertainty which is dominated by the uncertainties in the relative A coefficients (Figure 3) and in the relative atmospheric transmittance. The spectral region near 7300 cm^{-1} is a quasi-spectral void under the observing conditions as a result of strong absorption in the Ψ region of H_2O [(0$\hat{0}$0) → (101) and (000) → (200) absorption bands dominant]. An estimate of the rms noise level in this region yielded ≈3.8 x 10^{-4}, in the emission rate units of Figure 4. Thus the S/N ratio for the OH M (7,4) $P_1(3)$ transition is estimated to be ≈10^3. (An investigation of the background in the vicinity of the $P(13)$ transitions suggested the sidelobes of the $P_1(5)$ transitions in the OH M (8,5) band as the dominant source. The peak amplitude of these sidelobes was estimated to be <5% of the central maximum associated with the $P_1(13)$ transitions.)

In Figure 6, the OH(X,v' = 7) column populations associated with the spectra in Figure 4 are presented in the form of a Boltzmann plot to illustrate the nearly linear behavior for the low rotational levels and the pronounced departure from this low-N' slope for rotational levels with N' >10. We have included in the figure relative rotational populations in column for both the i = 1 ($^2\Pi_{3/2}$) and i = 2 ($^2\Pi_{1/2}$) substates of OH($X^2\Pi$, v' = 7). The observed ratio{CER [$P_1(13)$] / CER [$P_1(2)$]} ≈ 3.2 x 10^{-2} exceeds the IBD ratio by a factor of about 2 x 10^5. This result is similar to that reported by *Pendleton et al.* [1989*a*] for HLW conditions.

The low-N' portion of the distribution in Figure 6 is shown in more detail in Figure 7. The populations associated with rotational levels N' = 1, 2, and 3 were found to follow an IBD to within the experimental uncertainties in the data and analyses (≈1% level). This point is illustrated in Figure 8 which compares the pertinent OH M (7,4) P-branch spectra with synthetic spectra based on the IBD assumption and the transition probabilities of *Mies* [1974]. The least-squares procedure utilized in fitting the data [*Espy et al.*, 1988] yielded the value (170.5 ± 1.8) K for the effective "rotational temperature" (T_r) associated with this restricted low-N' portion of the OH(X,v' = 7) rotational population distribution. The error interval (≈±1%) is somewhat larger than expected on the basis of the very high S/N ratio of the data sample. In this case, a slight difference between the true instrumental line shape and that associated with the 'best-fit' synthetic spectra produces systematic residuals which dominate the error estimate.

It is clear from Figure 6 that the magnitude of the slope of the distribution curve in the low-N' region ($|m_1|$) is much larger than that in the high-N' region ($|m_2|$). An estimate of the ratio ($|m_1|/|m_2|$), based on a constrained value for the high-N' slope,

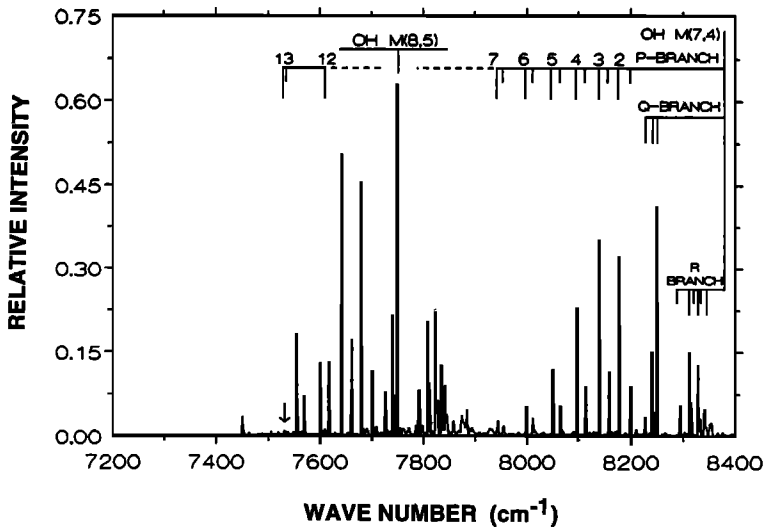

Fig. 4. Nightglow spectra in the 7200 - 8400 cm^{-1} region illustrating the rotational development in the OH M (7,4) P branches for mid-latitude, summer conditions. The $P(13)$ transitions are identified by the arrow near 7530 cm^{-1} and are shown in more detail in Figure 2.

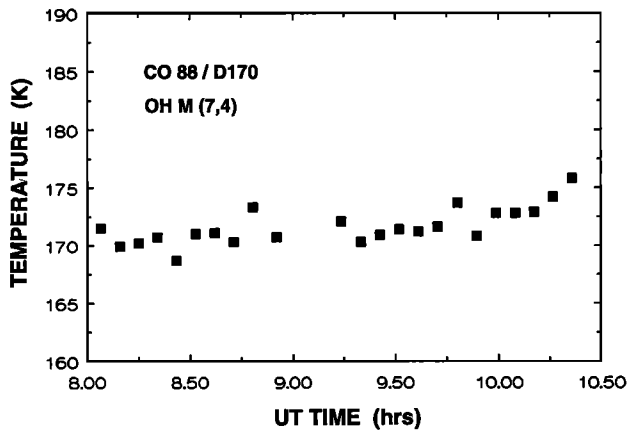

Fig. 5. OH M (7,4) rotational temperatures during the period 8.5 - 10.5 UT on June 19, 1988. The standard deviation of each 5.4-min sample is about 1.2 K. (The spectra shown in Figure 4 were obtained between 0800 and 0900 UT.)

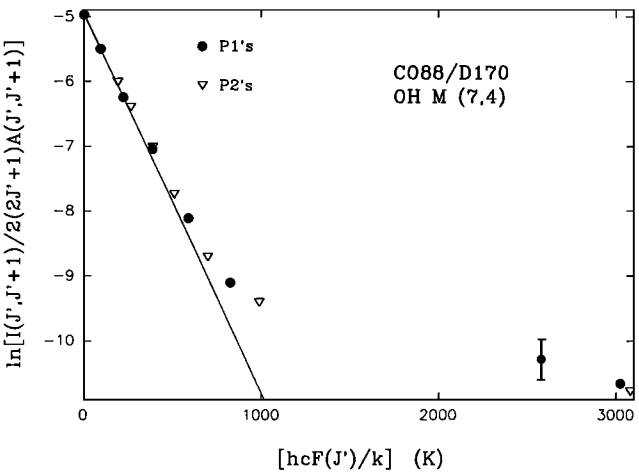

Fig. 6. Boltzmann plot for the OH M (7,4) P branches illustrating the quasi-LTE behavior for low N' and the strongly NLTE behavior for high N'.

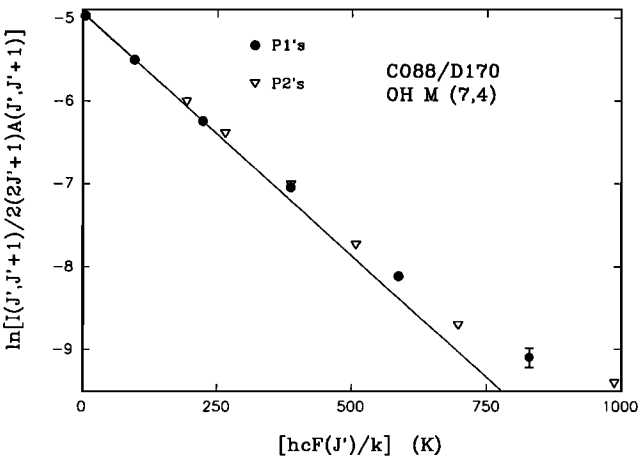

Fig. 7. Expanded plot of the low N' portion of Figure 6 showing the "breaking away" from the isothermal Boltzmann distribution.

yielded 9.8. Since the inverse of $|m_1|$ is consistent with a temperature of (170.5±1.8) K, the high-N' "population parameter," deduced from the ratio ($|m_1|/|m_2|$), is estimated to be ≈1700 K. The value of this high-N' population parameter is the same, to within the experimental uncertainties, as that deduced by *Pendleton et al.* [1989*a*] for HLW conditions. It should be noted that *Perminov et al.* [1991] have recently reported a temperature parameter of 1100 K in describing the rotatonal (intermediate - N') population distribution of the OH M (7,3) nightglow emissions. The rotational levels ($6 \leq N' \leq 9$) used in determining this parameter included two in the transition region (Figure 6). Hence it is not surprising that their effective value for this population parameter is of the same magnitude but somewhat smaller than that of the present study.

3.3. OH M (6,3) Band

As previously noted, this band with origin at ≈8744 cm^{-1} occurs in the "red" wing of the Φ absorption band of H_2O. Under typical MLS conditions several of the P branch transitions are strongly impacted by H_2O absorption. Hence, determination of the OH(X, v' = 6) rotational distribution in the MLS nightglow requires rather extensive differential extinction corrections. Despite this limitation, it is worth noting that the rotational development in the (6,3) P branches was observed to at least the $P(12)$ transitions under these conditions.

Some of the OH M (6,3) nightglow spectra obtained under HLW conditions are relatively free of H_2O absorption effects. In favorable cases, with ground-level temperatures near -35° C, it is possible to realize almost undistorted OH M (6,3) P_1-branch spectra. Under such conditions, the rotational development in this branch may be usefully followed to the $P_1(12)$ transition, as illustrated in Figure 9. The spectra in the figure were obtained using a relatively "hard" Kaiser-Bessel apodization which resulted in an ILS with principal side lobes of peak amplitude ≈10^{-3} that of the central maximum. Thus the OH M (6,3) $P_1(11)$ and $P_1(12)$ transitions, which occur near intense P-branch transitions in the (7,4) band, were more reliably identified and measured.

An example of the OH(X,v' = 6) rotational population

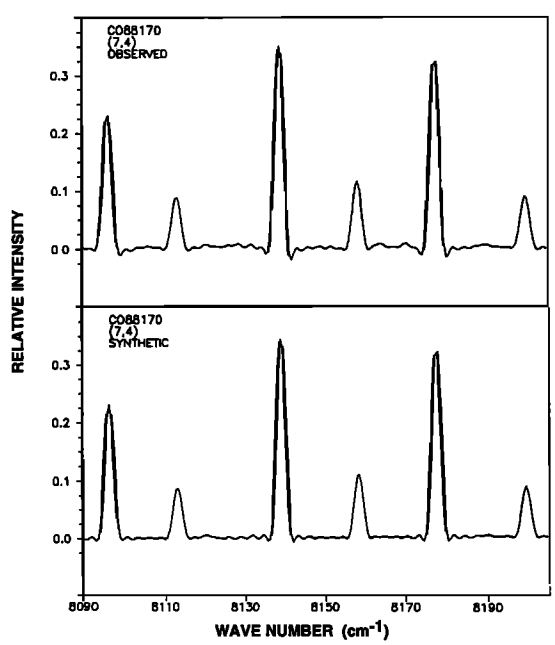

Fig. 8. Comparison of observed low-N' P branch transitions in the OH M (7,4) band with "best fit" synthetic spectra based on a Boltzmann model.

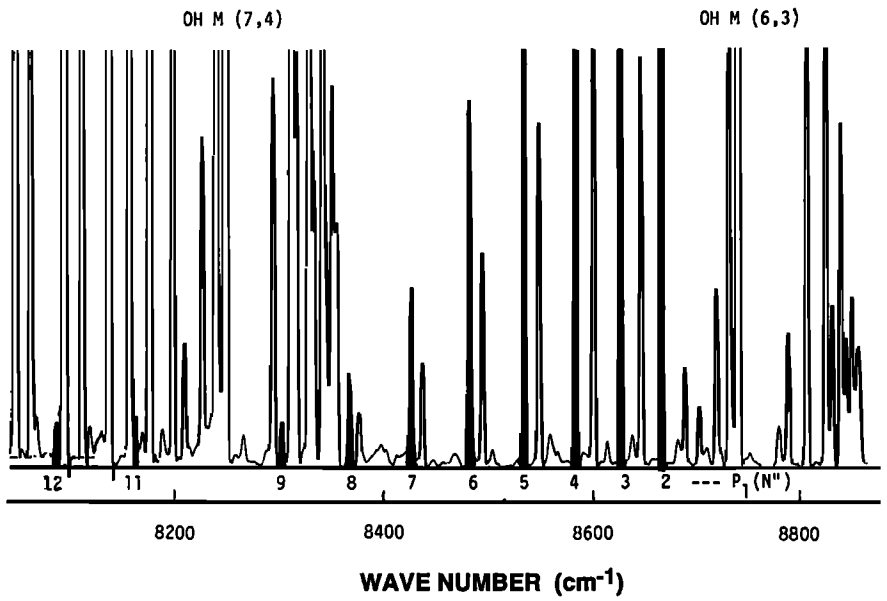

Fig. 9. Nightglow spectra in the OH M (6,3) region showing the rotational development in the P branches of this band under HLW conditions. The Kaiser-Bessel apodization function which was used reduced the principal side lobes on the ILS function to about 10^{-3} of the central maximum.

distribution in the HLW nightglow is shown in Figure 10. In this case, the low-N' ($N' \leq 4$) population distribution is adequately described by a temperature of ≈210 K, but a departure from this IBD becomes perceptible for $N'=5$ and severe for $N' \geq 8$. (The missing point at $N'=9$ results from the severe blending of the $P_1(10)$ transitions with the Q-branch transitions in the (7,4) band.) In comparing these results with those for the (7,4) band, obtained under the same conditions [*Pendleton et al.*, 1989*a*, Figure 3], we note that the low-N' distributions ($N' \leq 4$) are well described by the same rotational temperature T_r=(207.2±3.9) K. However, the high-N' populations for $v'=6$ appear to be systematically lower (relative to common IBD) than those for $v'=7$. This suggests that the high-N' levels for $v'=6$ are slightly "more relaxed" than their $v'=7$ counterparts.

3.4. OH M (3,1) Band

The rotational development in the P branches of the OH M (3,1) band has been followed to the $P_1(10)$ transitions near 6169 cm^{-1}. No attempt has been made to extend the observations to higher $P_1(N")$ transitions in this band, in part because of the unfavorable detection system response in the region <6000 cm^{-1} (≈1.7 μm) (the approximate long-λ detection limit for the LN_2-cooled intrinsic Ge detector).

An example of spectra used to identify the (3,1) $P_1(10)$ transitions is presented in Figure 11. A reference peak, which is dominated by the contribution from the (4,2) $P_2(4)$ Λ-doublet, is included in the figure. These results were obtained under the same MLS conditions as those which apply in Figure 6. An effective OH M (3,1) rotational temperature of (168.2±1.3) K was deduced from the transitions $P_1(N")$ with $N"=2$, 3, and 4 using the A coefficients of *Mies* [1974]. This result is in satisfactory accord with the value (170.5±1.8) K deduced from the same transitions in the OH M (7,4) band. Although the OH M (3,1) $P_1(10)$ emission rate in Figure 11 is relatively low, it exceeds the IBD value by a factor ~10^3. The observed ratio {CER[$P_1(10)$]/CER[$P_1(2)$]} was (2.6±0.5) x 10^{-2}, whereas the ratio predicted for an IBD distribution at 170 K is 3.4 x 10^{-5} using the transition probabilities of *Mies* [1974].

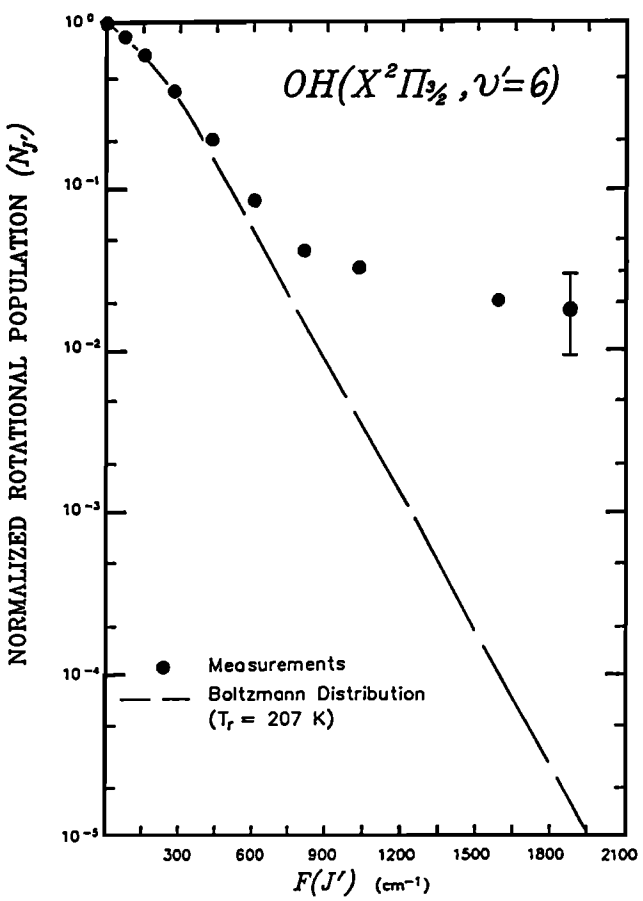

Fig. 10. OH(X,v'=6) rotational population distribution extending to N' = 11 for high-latitude, winter conditions.

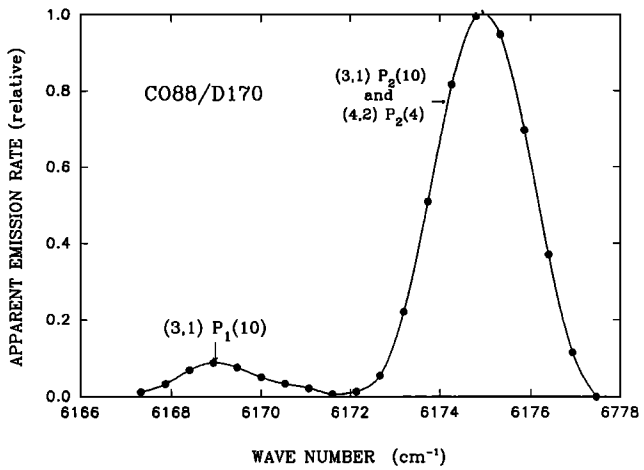

Fig. 11. Nightglow spectra in the 6170 cm^{-1} region for mid-latitude, summer conditions illustrating the presence of detectable OH M (3,1) $P_1(10)$ transitions.

3.5. OH M (4,2) and (5,3) R Heads

Persistent airglow features near 6503 cm^{-1} and 6165 cm^{-1} have been identified as the R branch heads in the OH M (4,2) and (5,3) bands, respectively. These features are illustrated in Figure 12, where they have been identified by arrows and labeled. The peak at ≈6503 cm^{-1} is conspicuous near the base of the $P_2(4)$ transitions of the OH M (3,1) band; whereas, the corresponding feature in the OH M (5,3) band forms a pedestal for the $P_1(4)$ transitions of the (4,2) band.

In Figure 13, the OH M (4,2) R heads are presented in more detail. The lower portion of the figure, which reflects a x23 vertical expansion of the designated region in the upper panel, provides tick marks at the positions of the R_1 (solid) and R_2 (dashed) transitions in the (4,2) R branches. Each tick mark identifies the mean position of a Λ-doublet, with the Λ-splitting ranging from ≈0.10 cm^{-1} for $R_1(1)$ to about 0.15 cm^{-1} for $R_1(15)$. The diagram was constructed using line-position data from *Maillard et al.* [1976]. These investigators realized a spectral resolution ≈0.01 cm^{-1} in their FTIR investigation of OH M Δv = 2 and 3 emissions from an oxyacetylene flame. The maximum uncertainty for the position of strong, unblended lines in the (4,2) R head region was estimated by the authors to be ± 0.0007 cm^{-1}. The high effective OH M rotational temperature in the flame (≈3100 K) ensured a significant population of the relatively high rotational levels which contribute to the emissions in the OH M (4,2) R head region. Here it should be noted that the OH M (4,2) R branch turning points occur at about 6504.9 cm^{-1} and 6504.0 cm^{-1} in the R_1 and R_2 transitions, respectively. These heads appear as a single feature under the resolution of the present investigation (≈2.6 cm^{-1}).

In Figure 14, we compare the HLW nightglow spectra in the (4,2) R head region with synthetic spectra based on an IBD model. The model accounts reasonably well for the very weak satellite transition near the base of the OH M (3,1) $P_1(3)$ transitions but fails to reproduce the more intense (4,2) R head feature. The high rotational transitions of interest in the P branches of the (4,2) band occur in the spectral region 5700-5900 cm^{-1} where the responsivity of the interferometric system is very low. As a result, we were unable to reliably assess the individual high-N' populations relative to those in low-N' region. An estimate of the total relative column population in the various rotational levels contributing to the R head feature (N_{RH}) is, however, possible since the A coefficients for the various transitions are nearly identical [*Mies*, 1974; *Langhoff et al.*, 1986; *Turnbull and Lowe*, 1989; *Nelson et al.*, 1990]. A typical value for the ratio [N_{RH} / $N(J' = 1.5)$] was found to be ≈ 0.05.

It is of historical interest to note that the OH M (4,2) R head feature in the terrestrial nightglow was apparently first observed by *Shemansky and Vallance Jones* [1961]. However, they were unable to identify the source of the "enhanced emission intensity at 1.538 μm," primarily as a result of the coarse spectral resolution (≥25 Å) used in their investigations. More recently, *Turnbull and Lowe* [1983] have identified the (4,2) R heads in their nightglow spectra obtained using much higher resolution ($\Delta\sigma \approx 2$ cm^{-1}), but they describe the feature as occurring at the base of the $P_1(3)$ lines in the (3,1) band. It is clear from Figure 13 and from the pertinent high-resolution

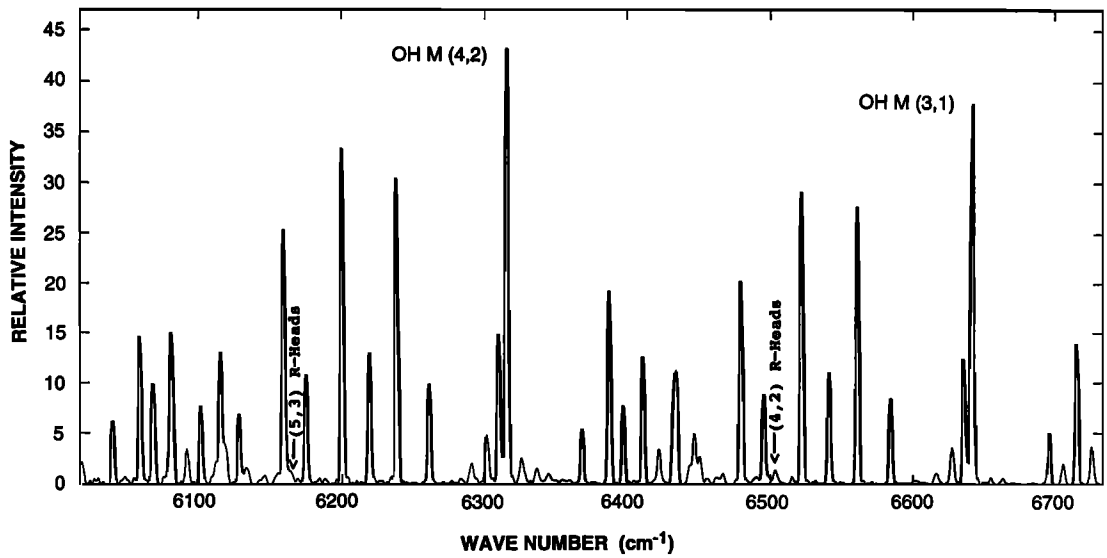

Fig. 12. Nightglow spectra in the region 6020 - 6735 cm^{-1} region for high-latitude, winter conditions showing the OH M (4,2) and (5,3) R head features.

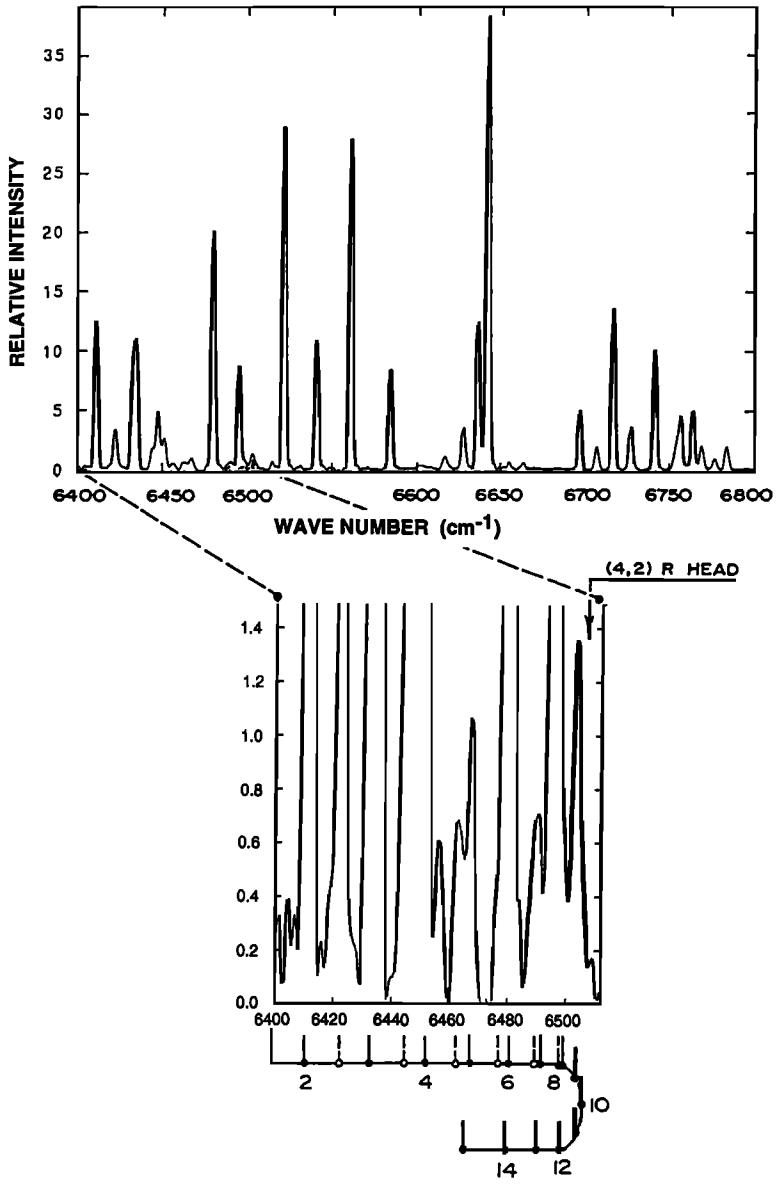

Fig. 13. (Upper) Enlarged view of the OH M (4,2) R head region illustrating its position at the base of the $P_2(4)$ transitions in the (3,1) band. (Lower) (4,2) R head region magnified vertically by a factor x23. The diagram at the bottom of the figure identifies the line positions in the R branches, as described in the text.

laboratory measurements of *Maillard et al.* [1976] that the (4,2) R heads are more appropriately associated with the spectral region near the base of the $P_2(4)$ lines in the (3,1) band. Our spectra show that the region near the base of the $P_1(3)$ lines is dominated on the low-frequency side by the OH M (3,1) $Q_{R12}(J_2" = 0.5)$ satellite transitions and on the high-frequency side by the $Q_{R12}(J_2" = 1.5)$ satellite transitions.

4. Discussion

4.1. Impact of Temperature Gradients

We have examined the impact of temperature gradients in the OH M source region on OH(X,v') rotational distributions under typical nightglow conditions and have found the associated distortion of the distributions to be too small to account for some of the key features of our observations. A MLS temperature profile based on the widely used MSIS model [*Hedin*, 1983, 1987] is shown in Figure 15. (The lower portion of this profile reflects a slight modification of the U.S. Standard Atmosphere (1976).) The profile was generated for summer solstice at mid-latitudes (40° N; 106° W) and magnetically-quiet conditions and is characterized by a minimum value of ≈166 K at about 92.5 km. The mean height of the OH M emission layer is ≈(87±3) km, and its mean thickness is ≈(9±3) km [*Baker and Stair*, 1988]. Hence the model kinetic temperature at the mean layer height is ≈175 K and the temperature interval corresponding to the mean layer thickness is ≈20 K. (The mean temperature gradient in this region is about -2.5 K/km.)

Under the assumption of LTE in rotation for OH(X,v'), we have partitioned the total v' population at altitude z according to the Boltzmann distribution

$$\eta_{v'J'}(z) = \eta_{v'}(z)\left\{\frac{2(2J'+1)\exp[-F(J')hc / kT(z)]}{Q_r}\right\}, \quad (2)$$

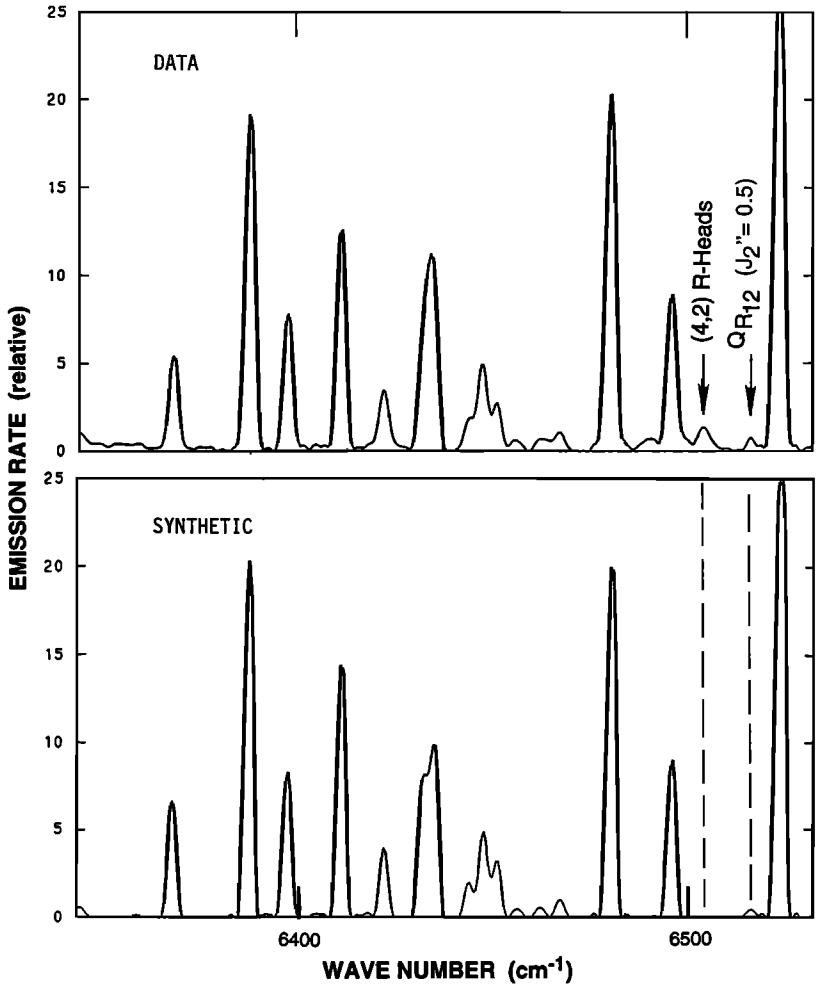

Fig. 14. Comparison of OH M (4,2) *R* head data with synthetic spectra based on the assumption of an IBD in rotation for the OH M (3,1) and OH M (4,2) emissions which contribute to this region.

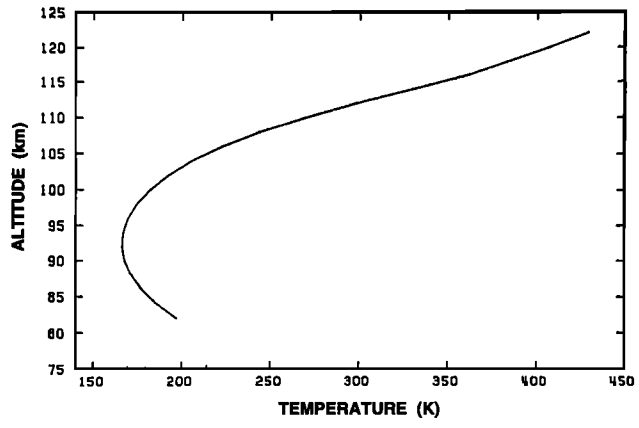

Fig. 15. Mid-latitude, summer temperature profile based on the MSIS model.

where

$$Q_r = \sum_{J'} 2(2J'+1) \exp\,[-F(J')hc/kT(z)]\ . \qquad (3)$$

Here, $J' = N' \pm 1/2$ identifies a particular rotational level in the manifold; $\eta_{v'}(z)$ is the total number density of OH(X,v') at altitude z; $F(J')$ is the rotational term value appropriate for vibrational level v' and h, c, and k are Planck's constant, the speed of light in vacuum, and Boltzmann's constant, respectively. Further, we have approximated $\eta_{v'}(z)$ by the Chapman function

$$\eta_{v'}(z) = \eta_{v'}(z_m) \exp\,[1 - Z - \exp\,(-Z)], \qquad (4)$$

where $Z = [(z-z_m)/H]$ with z_m the altitude at the peak of the layer and H a width factor (full layer width at one-half the maximum number density $\cong 2.5H$), and have imposed the requirement that $N_{v'} = 1$, with $N_{v'}$ the column density of OH(X,v') [integral of $\eta_{v'}(z)$ over altitude]. Under these conditions, the rotational manifold is normalized to unit total column population.

Reasonable ranges for the OH(X,v') layer height [82.5 km $\leq z_m \leq$ 92.5 km] and width (7.5 km $\leq 2.5H \leq$ 12.5 km) were adopted in the calculations [*Baker and Stair,* 1988]. It was necessary to extrapolate the MSIS temperature profile to lower altitudes in the case of the smaller values of z_m and the larger values of H. The extrapolation was realized by adjusting the slope of the MSIS profile near the lower boundary to yield a 75-km temperature of ≈200 K, in good accord with mid-latitude summer observations summarized in the U. S. Standard Atmosphere, 1976. For the specified conditions, with most of the OH(X,v') layer in a region where -2.5 K/km $\leq (dT/dz) \leq$ +2.5 K/km, the departure of predicted rotational distributions from an IBD type were very small (at most a few percent at $J' = 6.5$).

In sharp contrast, the MLS rotational distribution in Figure 6 exhibits a much more significant departure from the low-N'

IBD. This feature is illustrated in the bar-graph presentation in Figure 16 where the ratios of observed to predicted (IBD @ 170.7 K) relative emission rates in the OH M (7,4) $P_1(N'')$ transitions (N'' = 2-7) are shown. (Both distributions have been normalized to unity at the $P_1(2)$ transitions.) Two features of this illustration should be noted. First, the emission rates in the $P_1(N'')$ transitions with N'' = 2, 3, and 4 are well described by a single temperature (170.7±0.9) K. Second, the emission rates in transitions with $N'' \geq 5$ exceed the predicted values by factors which increase rapidly with N'' (1.11, 1.31, 1.97 for N'' = 5, 6, and 7, respectively). For the given conditions, the "breaking away" from the IBD is relatively abrupt, and the ratio of observed-to-predicted relative emission rates reaches a very large value ~10^5 for N''= 13.

Schubert et al. [1990] have recently shown that relatively large distortions of the OH(X,v') rotational distribution are possible if a large temperature gradient ($\gtrsim$10 K/km) extends throughout the OH M source region. Our computations confirm this general result. For example, the OH(X,v') rotational distribution was computed, as previously described, for a Chapman layer (FWHM ≅ 10 km ⇒ H = 4 km) in a region with a mean temperature gradient of ≈9 K/km and a layer-maximum temperature appropriate for a low-N' apparent temperature of ≈171 K.

Under these conditions, we find that temperatures computed in the manner described by *Shubert et al.* [1990] range from the low-N' value of 170.7 K to about 190 K for the apparent temperature determined from the population ratio $N(J' = 6.5)/N(J' = 5.5)$. In Figure 17, these computational results are compared with corresponding apparent temperatures deduced from successive $P_1(N'')$ pairs in the data set of Figure 6. Each point is plotted at the midpoint of the interval $(hc/k)\Delta F$ with ΔF the upper-state rotational term interval associated with the pair of transitions. It is evident from the figure that the apparent temperatures deduced from the data increase much more rapidly beyond the first two pairs than do those based on the model calculation. However, as expected on the basis of previous considerations, the first two points derived from the data correspond very closely to the same temperature (≈171 K), whereas the model results exhibit a distinct increase from point one to point two. The magnitude of this computed temperature increase varies systematically with the magnitude of the temperature gradient in the source region.

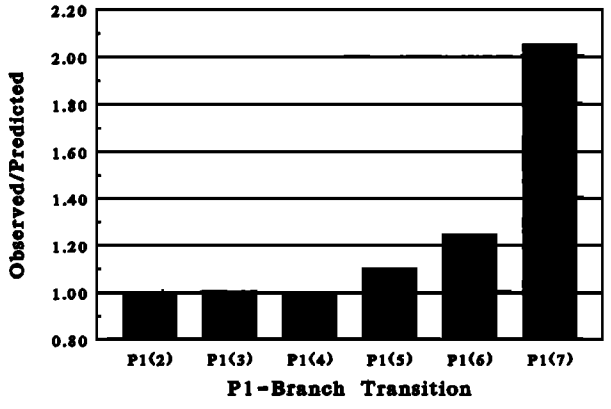

Fig. 16. Bar-graph presentation of the "breaking away" of the OH M (7,4) $P1$ branch transitions from the well-defined low N' IBD for the data in Figures 4, 6, and 7.

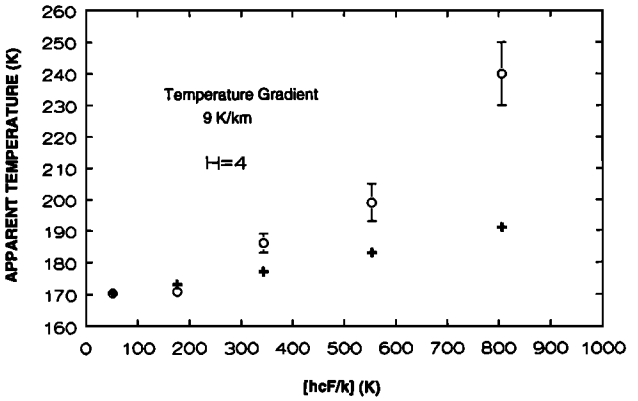

Fig. 17. Comparison of observed and predicted "breaking away" of the P branch rotational distribution from the quasi-isothermal low N' region. Apparent temperatures derived from the nonisothermal model described in the text (pluses). Apparent temperatures deduced from the data set illustrated in Figure 16 (open circles).

4.2. *OH M (4,2) R Heads and High-N' R-T Relaxation*

The presence of a readily observable OH M (4,2) R head in the nightglow spectra was unexpected since it reflects transitions with upper-state rotational levels in the range $9 \leq N' \leq 11$. Under the assumption of complete rotational-kinetic equilibrium at typical near-mesopause kinetic temperatures (especially for MLS conditions), these high-N' levels are expected to be insignificantly populated. Thus, our observations require a 'hot' high-N' population component. It is well established that the H + O_3 reaction forms rotationally 'hot' OH(X,v') principally in v' = 7-9 [*Charters et al.*, 1971; *Klenerman and Smith*, 1987]. However, the nascent rotational distribution will be greatly modified in radiative and collisional cascade to the v' = 4 level under typical nightglow conditions. Thus it is somewhat surprising that a significant high-N' population component remains at v' = 4.

Studies of rotational relaxation of hydrogen halides by Polanyi and co-workers [*Polanyi and Woodall*, 1972; *Ding and Polanyi*, 1975] suggest that the high-N' levels of vibrationally-excited OH(X) should relax much more slowly than the low-N' levels. [Note that the rotational energy level separation $E(N' + 1) - E(N')$ for OH($X\,^2\Pi$,v' = 4) is ≈0.5 kT and ≈2.6 kT for N' = 1 and N' = 11, respectively, when T = 200 K.] This 'differential relaxation' could conceivably account for the non-thermal, high-N' population component. The total OH(X,v' = 4) rotational distribution apparently consists of the well-established quasi-LTE low-N' component, which contains most of the population, and a NLTE high-N' component, which is presumably a remnant of the highly NLTE nascent rotational distribution associated with the high vibrational levels. (It should be noted that the net effect of radiative relaxation is to "pump" the nascent rotational distribution to higher J' values as a result of the dominance of P branch ($J' \rightarrow J' + 1$) transitions in the radiative decay of OH(X,v',J').)

Sung and Setser [1978] have shown that the relaxation of high rotational levels ($J' \geq 10$) of HF($X^1\Sigma^+$), which has rotational spacings similar to those of OH($X^2\Pi$), is slow even at 1 Torr buffer-gas (argon) pressure. In this connection, they demonstrated that a very significant high-J' population component remained despite an estimated 4 x 10^3 HF(X,v',J') - Ar collisions. Thus while the number of collisions during one rotational relaxation time (Z_{rot}) is known to be ~10 for the lower rotational levels of the hydrogen halides [*Breazeale and*

Kneser, 1960] and of OH [*Kistiakowsky and Tabbutt*, 1959], it would appear that Z_{rot} for the high rotational levels is much larger. The well-established "exponential energy gap law" [*Ding and Polanyi*, 1975; *Sung and Setser*, 1978] for the probability of state-to-state rotational transitions in bimolecular collisions appears to account for most of the general features of the observed behavior.

5. Conclusions

The OH(X,v' = 7) rotational distribution under MLS conditions is frequently characterized by a low-N' component (N' = 1, 2, and 3) which is well described (≈1% level) by a single temperature. However, a rapid "breaking away" from the low-N' IBD becomes readily detectable at N' = 4. The excess population in high-N' levels becomes extreme at N' = 12, with the observed value typically a factor in the range 10^4 - 10^5 larger than the IBD prediction.

An excess high-N' population persists in lower vibrational levels of OH(X) under typical nightglow conditions, as evidenced by the observation of P branch transitions extending to $P_1(10)$ in the (3,1) band and $P_1(12)$ in the (6,3) band. High-N' population components were also inferred for v' = 4 and 5 as a result of the readily detectable R heads in the (4,2) and (5,3) bands.

The observation of a nearly isothermal (≈1% level) low-N' (N' = 1, 2, and 3) OH(X,v' = 7) population component in the MLS nightglow coupled with the rapid "breaking away" from this distribution for levels with $N' \geq 4$ appear to be inconsistent with temperature gradients in the source region as the dominant mechanism. However, additional related observations obtained under well-defined atmospheric conditions are urgently needed to unequivocally establish the relative contributions of source region temperature gradients and NLTE to the observed departures from the low-N' IBD region.

Acknowledgments. This study was supported primarily by the Air Force Office of Scientific Research through the MAPSTAR Program of the Air Force Geophysics Laboratory (now Geophysics Directorate of Phillips Laboratory). However, some of the data used in the investigation was acquired through grants to Utah State University from the National Science Foundation (ATM-8411329 and ATM-8542127). The significant contributions of P. Mace of Utah State University to the acquisition and documentation of data are gratefully acknowledged. The authors also acknowledge the support and encouragement of E. Dewan and R. O'Neil of Phillips L.

The Editor thanks E. J. Llewellyn and another for their assistance in evaluating this paper.

References

Baker, D. J., Field-widened interferometers for Fourier spectroscopy, in *Spectrometric Techniques*, edited by G. Vanasse, pp.71-106, Academic, San Diego, Calif., 1977.

Baker, D. J., and A. T. Stair, Jr., Rocket measurements of the altitude distributions of the hydroxyl airglow, *Phys. Scr., 37*, 611-622, 1988.

Bates, D. R., Airglow and Auroras, in *Applied Atomic Collision Physics*, edited by H. S. W. Massey and D. R. Bates, pp.152-213, Academic, San Diego, Calif., 1982.

Benedict, W. S., E. K. Plyler, and C. J. Humphreys, The emission spectrum of OH from 1.4 to 1.7 μ, *J. Chem. Phys., 21*(3), 398-402, 1953.

Breazeale, M. A., and H. O. Kneser, Rotational relaxation in hydrogen chloride, *J. Acoust. Soc. Am., 32*, 885-886, 1960.

Chamberlain, J. W., *Physics of the Aurora and Airglow*, 704 pp., Academic, San Diego, Calif., 1961.

Charters, P. E., R. G. MacDonald, and J. C. Polanyi, Formation of vibrationally excited OH by the reaction H + O_3, *Appl. Opt., 10*, 1747-1754, 1971.

Coxon, J. A., Optimum molecular constants and term values for the $X^2\Pi(v \leq 5)$ and $A\,^2\Sigma^+$ ($v \leq 3$) sates of OH, *Can. J. Phys., 58*, 933-949, 1980.

Coxon, J. A., and S. C. Foster, Rotational analysis of hydroxyl vibration-rotation emission bands: Molecular constants for OH $X^2\Pi$, $6 \leq v' \leq 10$, *Can. J. Phys., 60*, 41-48, 1982.

Dick, K. A., Short time-interval spectrometric hydroxyl emission studies, *Ann. Geophys., 28*, 149-153, 1972.

Ding, A. M. G., and J. C. Polanyi, Energy transfer as a function of collision energy, I, Collision partners: Hydrogen halides + inert gases, hydrogen halides, H_2S, and propane, *Chem. Phys., 10*, 39-49, 1975.

Espy, P. J., C. R. Harris, A. J. Steed, J. C. Ulwick, R. H., Haycock, and R. Straka, Rocketborne interferometer measurement of infrared auroral spectra, *Planet. Space Sci., 36*(6), 543-551, 1988.

Gattinger, R. L., and A. Vallance Jones, Observation and interpretation of hydroxyl airglow emissions, in *Physics and Chemistry of Upper Atmospheres*, edited by B. M. McCormac, pp. 184-192, D. Reidel, Hingham, Mass., 1973.

Harrison, A. W., E. J. Llewellyn, and D. C. Nicholls, Night airglow hydroxyl rotational temperatures, *Can. J. Phys., 48*, 1766-1768, 1970.

Harrison, A. W., W. F. J. Evans, and E. J. Llewellyn, Study of the (4,1) and (5,2) hydroxyl bands in the night airglow, *Can. J. Phys., 49*, 2509-2517, 1971.

Harrison, A. W., and D. J. W. Kendall, Airglow hydroxyl doublet ratio temperatures, *J. Geophys. Res., 78*(22), 4697-4701, 1973.

Haycock, R. H., and D. J. Baker, Infrared prism interferometer-spectrometer using a gas lubricated drive bearing, *Infrared Phys., 14*, 259-269, 1974.

Hedin, A. E., A revised thermospheric model based on mass spectrometer and incoherent scatter data: MSIS-83, *J. Geophys. Res., 88*, 10170-10188, 1983.

Hedin, A. E., MSIS-86 thermospheric model, *J. Geophys. Res., 92*, 4649-4662, 1987.

Kistiakowsky, G. B., and F. D. Tabbutt, Gaseous detonations, XII, Rotational temperatures of the hydroxyl free radicals, *J. Chem. Phys., 30*(2), 577-581, 1959.

Klenerman, D., and I. W. M. Smith, Infrared chemiluminescence studies using a SISAM spectrometer. Reactions producing vibrationally excited OH, *J. Chem. Soc., Faraday Trans. 2, 83*, 229-241, 1987.

Kvifte, G., Temperature measurements from OH bands, *Planet. Space Sci., 5*, 153-157, 1961.

Langhoff, S. R., H-J. Werner, and P. Rosmus, Theoretical transition probabilities for the OH Meinel system, *J. Mol. Spectrosc., 118*, 507-529, 1986.

Llewellyn, E. J., and B. H. Long, The OH Meinel bands in the airglow — the radiative lifetime, *Can. J. Phys., 56*, 581-586, 1978.

Maillard, J. P., J. Chauville, and A. W. Mantz, High-Resolution Emission Spectrum of OH in an Oxyacetylene Flame from 3.7 to 0.9 μm, *J. Mol. Spectrosc., 63*, 120-141, 1976.

McPherson, D. H., and A. Vallance Jones, A study of the latitude dependence of OH rotational temperatures for Canadian stations, *J. Atm. Terr. Phys., 17*, 302-308, 1960.

Meinel, A. B., Hydride emission bands in the spectrum of the night sky, *Astrophys. J., 111*, 207, 1950*a*.

Meinel, A. B., OH emission bands in the spectrum of the night sky, I, *Astrophys. J., 111*, 555-564, 1950*b*.

Meinel, A. B., OH emission bands in the spectrum of the night sky, II, *Astrophys. J., 112*, 120-130, 1950*c*.

Mies, F. H., Calculated vibrational transition probabilities for OH($X^2\Pi$), *J. Mol. Spectrosc., 53*, 150-188, 1974.

Nelson, D. D., Jr., A. Schiffman, D. J. Nesbitt, J. J. Orlando, and J. B. Burkholder, H + O_3 Fourier-transform infrared emission and laser absorption studies of OH($X^2\Pi$) radical: An experimental dipole moment function and state-to-state Einstein A coefficients, *J. Chem. Phys., 93*(10), 7003-7019, 1990.

Neuber, R., P. von der Gathen, and U. von Zahn, Altitude and temperature of the mesopause at 69° N latitude in winter, *J. Geophys. Res., 93*, 11093-11101, 1988.

Nicholls, D. C., M. Sci. thesis, Univ. of Saskatchewan, Saskatchewan, Canada, 1971.

Nicholls, D. C., W. F. J. Evans, and E. J. Llewllyn, Collisional relaxation and rotational intensity distributions in spectra of aeronomic interest, *J. Quant. Spectrosc. Radiat. Transfer, 12*, 549-558, 1972.

Pendleton, W., Jr., P. Espy, D. Baker, A. Steed, M. Fetrow, and K.

Henriksen, Observation of OH Meinel (7,4) $P(N'' = 13)$ transitions in the night airglow, *J. Geophys. Res.*, *94*, 505-510, 1989*a*.

Pendleton, W., P. Espy, J. Hartman, M. Fetrow, and G. Sivjee, Nitrogen I 3F ($^2P^o \rightarrow {}^2D^o$) emissions in the aurora, *J. Geophys. Res.*, *94*, 2594-2604, 1989*b*.

Perminov, V. I., A. I. Semenov, and N. N. Shefov, Non-equilibrium population distributions of the higher rotational levels of the hydroxyl molecule in the nocturnal mesopause, in *Proc. 18th Ann. Mtng. of the Studies of the Upper Atmos. by Opt. Methods*, *18*, 56, 1991.

Polanyi, J. C., and K. B. Woodall, Energy distribution among reaction products, VI, F + H_2, D_2, *J. Chem. Phys.*, *57*, 1574-1586, 1972.

Roychoudhury, D. K., Airglow technique to compute mesospheric temperature and integrated water vapor concentration of the atmosphere, M. Sci. thesis, Utah State Univ., Logan, 1983.

Schubert, G., and R. L. Walterscheid, Wave-driven fluctuations in OH nightglow from an extended source region, *J. Geophys. Res.*, *93*, 9903-9915, 1988.

Schubert, G., R. L. Walterscheid, J. H. Hecht, and G. G. Sivjee, Temperature gradients at mesopause heights inferred from OH nightglow data, *J. Geophys. Res.*, *95*, 19061-19067, 1990.

Shefov, N. N., On determination of the rotational temperatures of OH bands, in *Spectral, Electrophotometrical, and Radar Researches of Aurora and Airglow*, edited by V. I. Krassvosky, pp. 1-7, Academy of Sciences, Moscow, 1961.

Shefov, N. N., Hydroxyl emission, *Ann. Geophys.*, *28*, 137-143, 1972*a*.

Shefov, N. N., Remarks on the OH Rotational Temperature in the Night Glow, *Can. J. Phys.*, *50*, 1225-1226, 1972*b*.

Shemansky, D. E., and A. Vallance Jones, New measurements of the night airglow in the 1.5 μ region, *J. Atmos. Terr. Phys.*, *22*, 166-175, 1961.

Sivjee, G. G., K. A. Dick, and P. D. Feldman, Temporal variation in night-time hydroxyl rotational temperature, *Planet. Space Sci.*, *20*, 261-269, 1972.

Sivjee, G. G., and R. M Hamwey, Temperature and chemistry of the polar mesopause OH, *J. Geophys. Res.*, *92*, 4663-4672, 1987.

Steed, A. J., Field-widened interferometry at Utah State University (USU), *J. Soc. Photo Opt. Instrum. Eng.*, *191*, 2-14, 1979.

Steed, A. J., and D. J. Baker, Night sky spectral emission measurements (λ 0.9 - 2.3 μm) using a field-widened interferometer spectrometer, *Appl. Opt.*, *18*(20), 3386-3389, 1979.

Steed, A. J., D. J. Baker, B. Y. Bartchi, and A. T. Stair, Jr., Recent auroral measurements using a field-widened interferometer spectrometer, *J. Soc. Photo. Opt. Instrum. Eng.*, *289*, 202-205, 1981.

Sung, J. P., and D. W. Setser, Observation of high rotational levels of HF formed by chemical reaction in one torr of argon buffer gas, *J. Chem. Phys.*, *69*(8), 3868-3869, 1978.

Turnbull, D. N., and R. P. Lowe, Vibrational population distribution in the hydroxyl night airglow, *Can. J. Phys.*, *61*, 244-250, 1983.

Turnbull, D. N., and R. P. Lowe, New hydroxyl transition probabilities and their importance in airglow studies, *Planet. Space Sci.*, *37*(6), 723-738, 1989.

Vallance Jones, A., The infrared spectrum of the airglow, *Space Sci. Rev.*, *15*, 355-400, 1973.

Wallace, L., The OH nightglow emission, *J. Atmos. Sci.*, *19*(1), 1-16, 1962.

P. J. Espy, M. R. Hammond, and W. R. Pendleton, Jr., Department of Physics and Space Dynamics Laboratory, Utah State University, Logan, UT 84322-4415.

(Received September 27, 1991;
revised March 10, 1993;
accepted March 13, 1993.)